Anat Embryol (2005) 210: 447–453
DOI 10.1007/s00429-005-0034-4

ORIGINAL ARTICLE

René Hurlemann · Andreas Matusch
Simon B. Eickhoff · Nicola Palomero-Gallagher
Philipp T. Meyer · Christian Boy · Wolfgang Maier
Karl Zilles · Katrin Amunts · Andreas Bauer

Analysis of neuroreceptor PET-data based on cytoarchitectonic maximum probability maps: a feasibility study

Published online: 27 September 2005

Abstract Three-dimensional maximum probability maps (MPMs) of cytoarchitectonically defined cortical regions based on postmortem histological studies have recently been made available in the stereotaxic reference space of the Montreal Neurological Institute (MNI) single subject template. This permits the use of cytoarchitectonic maps for the analysis of functional in vivo datasets, including neuroreceptor positron emission tomography (PET) studies. In this feasibility study, we used 5-hydroxytryptamine 2A (5-HT_{2A}) receptor PET to test the applicability of maximum cytoarchitectonic probability maps for quantitative analysis. As the outcome parameter, we extracted local distribution volume ratios (DVRs) from 19 cytoarchitectonically defined volumes of interest (VOIs) per hemisphere from five healthy subjects. The experimental design included a forward ('PET to atlas' normalization) and a backward ('atlas to PET' normalization) procedure to double-check the stability of transformation and overlay. Resulting DVRs were compared with receptor densities (RDs) obtained from postmortem [^{3}H]ketanserin autoradiography of multiple areas. Correlations between the bi-directional normalization procedures ($r = 0.89$; 38 VOIs) as well as between in vivo and vitro data (nine VOIs; $r = 0.64$ and $r = 0.47$ for forward and backward procedure, respectively) suggest that the implementation of cytoarchitectonic maximum probability maps is a promising method for an accurate and observer-independent analysis of neuroreceptor PET data.

Keywords 5-HT_{2A} · [^{18}F]Altanserin PET · Probabalistic · Atlas · Cytoarchitecture

R. Hurlemann · A. Matusch · S. B. Eickhoff
N. Palomero-Gallagher · P. T. Meyer · C. Boy
K. Zilles · K. Amunts · A. Bauer (✉)
Brain Imaging Center West, Institute of Medicine,
Research Center Jülich, Jülich, Germany
E-mail: an.bauer@fz-juelich.de
Tel.: +49-2461-614288
Fax: +49-2461-618273

W. Maier · R. Hurlemann
Department of Psychiatry, University of Bonn,
Bonn, Germany

K. Zilles
C & O Vogt Institute for Brain Research,
University of Duesseldorf, Duesseldorf, Germany

Introduction

Accurate identification of cortical regions based on macroscopical topography is limited by the fact that macroscopical structures neither reflect the microscopical parcellation of the cerebral cortex nor its functional organization (Zilles et al. 2002). Therefore, a cytoarchitectonic probabalistic atlas of the human cerebral cortex based on postmortem histological studies has been developed. Probabilistic maps of the motor (Geyer et al. 1996), somatosensory (Geyer et al. 1999; Grefkes et al. 2001), auditory (Morosan et al. 2001, 2005), and visual cortex (Amunts et al. 2000), as well as of Broca's region (Amunts et al. 1999), opercular regions (Eickhoff et al. 2005a, b), and intraparietal areas (Choi et al. 2002) have been created. These data rely on an observer-independent analysis of the cortical architecture of 10 postmortem brains, which were sectioned into 20-µm slices. Borders between cortical areas were identified by using the grey-level index (GLI) as a measure of the volume fraction occupied by cell bodies (Schleicher et al. 1999). Resulting cytoarchitectonic data were 3D-reconstructed and warped onto the Montreal Neurological Institute (MNI) single subject reference brain (Collins et al. 1994; Evans et al. 1993; Holmes et al. 1998) to enable anatomical labelling in stereotaxic space (Mohlberg et al. 2003; online at http://www.bic.mni.mcgill.ca/cytoarchitectoznic/ and http://www.fz-juelich.de/ime/ime_probability_maps/). Equiprobability contures indicate the likelihood (e.g., 10, 20,...,100%) of a given voxel being localized in a cytoarchitectonically defined area.

Such cytoarchitectonic probability maps are typcially characterized by an overlap across areas. Based on these maps, maximum probability maps (MPMs) have been

calculated, which assign to every voxel the maximum probability that it is localized in a particular anatomical area. They are, therefore, more suitable for application in PET data analysis. In cases of overlap, isoprobability lines distinguish separate areas. In the remaining voxels, MPMs are based on 40% probability contures (Eickhoff et al. 2004). Note that in the set of regions thus far available, a minimum overlap and sparing of voxels between neighbouring regions occurs with 40% probability maps. MPMs permit the definition of continuous, non-overlapping volumes of interest (VOIs), which can be used in the analysis of PET data sets. The MPMs used in this study were as follows: Brodman area (BA)1, BA2, BA3a, BA3b, BA4a, BA4p, and BA6 of the sensorimotor cortex, V1 (homologue to BA17), V2 (homologue to BA18) of the visual cortex, TE1.0 (part of BA41), TE1.1 (part of BA41), TE3 (part of BA22) of the auditory cortex, BA44 (part of Broca's area), BA45 (part of Broca's area), OP1, OP2, OP3, OP4 (OP1–OP4 correspond to the functionally defined secondary somatosensory cortex), IP1 (ventral intraparietal area), and IP2 (anterior intraparietal area).

The focus of the present study was to test the feasibility of MPMs for the regional analysis of neuroreceptor PET data. The cerebral 5-HT_{2A} receptor (5-HT_{2A}R) was investigated using [^{18}F]altanserin for PET and its keto-analogue [^{3}H]ketanserin for in vitro studies, respectively (available online at http://www.-fz-juelich.de/ime/index.php?index = 155). Specifically, we examined (a) the stability of the applied image analysis, as determined by doublechecking a forward procedure ('PET to atlas' normalization) to a backward procedure ('atlas to PET' normalization), (b) the selection of those MPMs that permit a stable PET analysis, and (c) an in vivo–in vitro comparison of PET and autoradiography data.

Methods and materials

Subjects

Study protocols were approved by the Ethics Committee of the Medical Faculty of the University of Bonn, Germany, and the German Federal Office for Radiation Protection. Five healthy volunteers (two females, three males; mean age 23 ± 1.8 years; range 21–25 years) participated after giving written informed consent. Subjects were free of any medical, neurological, and psychiatric condition, including head injury, alcohol, or substance abuse. Individual high-resolution magnetic resonance imaging (MRI) was performed on a 1.5T vision scanner (Siemens, Erlangen, Germany) using a 3D T1-weighted magnetization-prepared rapid-acquisition gradient-echo sequence (MP-RAGE; voxel size $1\times1\times1$ m^3). Human postmortem brains were obtained from the body donor program of the Anatomical Institute, Heinrich-Heine-University Düsseldorf, Germany. Brains from three donors (one female, 77 years; two males, 54 and 77 years) without a history of neurological or psychiatric illness were selected for in vitro receptor autoradiography. A detailed survey of the experimental procedures has been given by Zilles et al. (2002). A total of 16 postmortem brains were embedded in paraffin, cut, stained for cell bodies and analysed with respect to cytoarchitecture at different cortical areas. For each area a subset of 10 brains was available to create cytoarchitectonic, probabilistic maps (Zilles et al. 2002).

PET imaging

Radiosynthesis of [^{18}F]altanserin was performed at the Institute of Nuclear Chemistry, Research Center Jülich, according to Lemaire et al. (1991), followed by high-performance liquid chromatography (HPLC) purification (Hamacher et al. 1995) with a radiochemical yield of ≈30% and a radiochemical purity of >99%. At the time of injection the mean specific radioactivity was 85 GBq/μmol (range: 27–138 GBq/μmol). PET measurements were performed in 3D mode on a Siemens ECAT EXACT HR+ scanner (Siemens-CTI, Knoxville, TN, USA). Scatter from outside the field of view was reduced by inserting a lead ring into the scanner gantry. A 10-min transmission scan (^{68}Ge/^{68}Ga) was obtained for attenuation correction. A bolus (20 s) with a mean radioactivity of 241 MBq (range 214–260 MBq) of [^{18}F]altanserin in 10-ml saline was injected intravenously. Dynamic data were collected in 24 frames over a 60-min period starting at time of injection. PET data were corrected for randoms, scatters, and attenuation, Fourier rebinned into 2D sinograms, reconstructed by filtered backprojection (Shepp filter, 2.5-mm width) with a voxel size of $2\times2\times2.43$ mm^3 (63 slices), and decay-corrected.

Image analysis

Individual MRI data sets were oriented to the anterior commissure–posterior commissure line using a 3D image registration software (MPITool, ATV Co., Germany). Subsequently, a summed PET image (5–60 min) was co-registered to the realigned MRI, and co-registration parameters were applied to each PET frame. Image analysis was based on a set of 2×19 VOIs defined by 3D MPMs implemented in a supplementary toolbox (Eickhoff et al. 2004) for Statistical Parametric Mapping (SPM2, Wellcome Department of Imaging Neuroscience, Institute of Neurology, UCL, London, UK, online at http://www.fil.ion.ucl.ac.uk/spm).

Normalization was performed bi-directionally using SPM2. In a forward procedure, individual dynamic PET images were spatially normalized to the MNI single subject template. Normalization parameters were obtained from co-registered individual MRI volumes (voxel size $2\times2\times2$ mm^3). The MPM-VOI set was imported into a PET-analysis specific software

(PMOD, V2.5, PMOD Group, Switzerland) and superimposed onto each normalized dynamic PET frame to generate time–activity curves (TACs). In a backward procedure, the single subject template, and thus the MPM-VOI set, was spatially normalized to individual MRI volumes. TACs were generated from each individual's native dynamical PET series. In both the forward and the backward procedure the cerebellum served as a reference region assuming that cerebellar [^{18}F]altanserin uptake mostly reflects free and non-specifically bound ligand (Pazos et al. 1987). For kinetic analyses, Logan's non-invasive graphical analysis (GA, Logan et al. 1996) was applied. The relative distribution volume ratio (DVR) of [^{18}F]altanserin given by the slope of the linear part of the GA plot (start of linearisation at 15 min) was used as an outcome parameter. DVR is directly related to the maximum number of receptors available for ligand binding (B_{max}'): DVR = 1 + $f_2 \times B_{max}$'/KD (f_2, tissue fraction of free ligand; KD, dissociation constant of the receptor–ligand complex) (Abi-Dargham et al. 1994; Laruelle et al. 1994).

To enable comparison with autoradiography data, volume weighted averages of corresponding left and right hemispheric VOIs were calculated. 5-HT_{2A}receptor densities (fmol/g protein) yielded from postmortem [^{3}H]ketanserin autoradiography of three subjects were measured in 11 cytoarchitectonicaly identified regions based on adjacent Nissl stained sections (Zilles et al. 2002). Autoradiography data were not available for all regions of every subject. Receptor density values differed between individuals in range and offset, but not in the rank-order of regions. Individual autoradiography data were therefore linearly normalized to the mean receptor density values available for six regions in each subject. Spearman's rank correlation coefficient was calculated between in vivo DVR values obtained from [^{18}F]altanserin PET and normalized receptor density values obtained from in vitro [^{3}H]ketanserin autoradiography.

Results

PET analysis

Visual inspection confirmed accurate fit of the MPMs to the functional PET data for both normalization procedures (Fig. 1), except for BA3a, which was excluded from further analysis because of its artificial white matter position. DVRs obtained from both the forward and the backward procedures are given in Table 1. Areas BA1, BA4, and BA6 showed the lowest DVRs, while the temporal subarea TE1.0, the opercular areas OP1, OP4, the anterior intraparietal area (IP2), BA44, and BA45 had high values. There is no evidence for a systematic DVR difference between left and right hemispheres.

Comparison of the procedures for bimodal overlay

The relative DVR difference between the forward and backward procedures was low as given in Table 1, exceeding 5% only in BA1, BA4p, IP1, OP2 bilaterally, as well as in the left BA2 and OP3. DVRs were highly correlated between the forward and backward procedures ($r = 0.89$). Iterative removal of the smallest region (Table 1) resulted in a correlation coefficient exceeding 0.95 for regions larger than 3.5 ml and 0.975 for regions larger than 8 ml (Fig. 2).

In vivo–in vitro correlation

An overview of correlation coefficients is given in Table 2. In vivo–in vitro rank correlations exceeded 0.46 in all subjects with one exception (subject 4), which was also the outlier of the interprocedure correlation, suggesting a suboptimal overlay of PET and atlas in this individual. Figure 3 depicts the relation of mean DVRs and autoradiography values. Autoradiographic data of areas 44 and 45 of Broca's region were available only from one subject and, therefore, excluded. In vivo–in vitro correlation analysis from the remaining nine regions yielded $r = 0.64$ (forward procedure) and $r = 0.47$ (backward procedure), respectively.

Discussion

In the present study, we tested the applicability of cytoarchitectonic MPMs to generate TACs for VOI-based neuroreceptor PET analysis. The study design comprised a forward and a backward procedure to control for possible confounding factors (e.g., recalculation of pixel values in the forward procedure, non-reversible operations, observer-dependent bias) resulting from spatial normalization. In general, different methods exist to extract TACs from VOIs: If mean activities across each VOI are measured, normalization should preserve pixel-wise mean activity. Conversely, if the focus is on summed activity within a VOI, normalization should preserve total activity. In our analysis, normalization was done the first way, and 2×19 VOIs were compared with each other and to in vitro autoradiography. We found almost identical DVRs following the forward and backward procedures. For spatial transformation into stereotaxic space, we applied the non-affine spatial normalization routine implemented in SPM2, which allows the use of unsegmented native structural MRIs. Alternative normalization protocols (e.g., Mohlberg et al. 2003) require elaborate pre-processing including segmentation and/or skull stripping of the structural MRI datasets.

In [^{18}F]altanserin PET, the gross uptake of radioactivity and the derived DVRs do not directly reflect 5-HT_{2A} receptor density, as they are confounded by (a) the

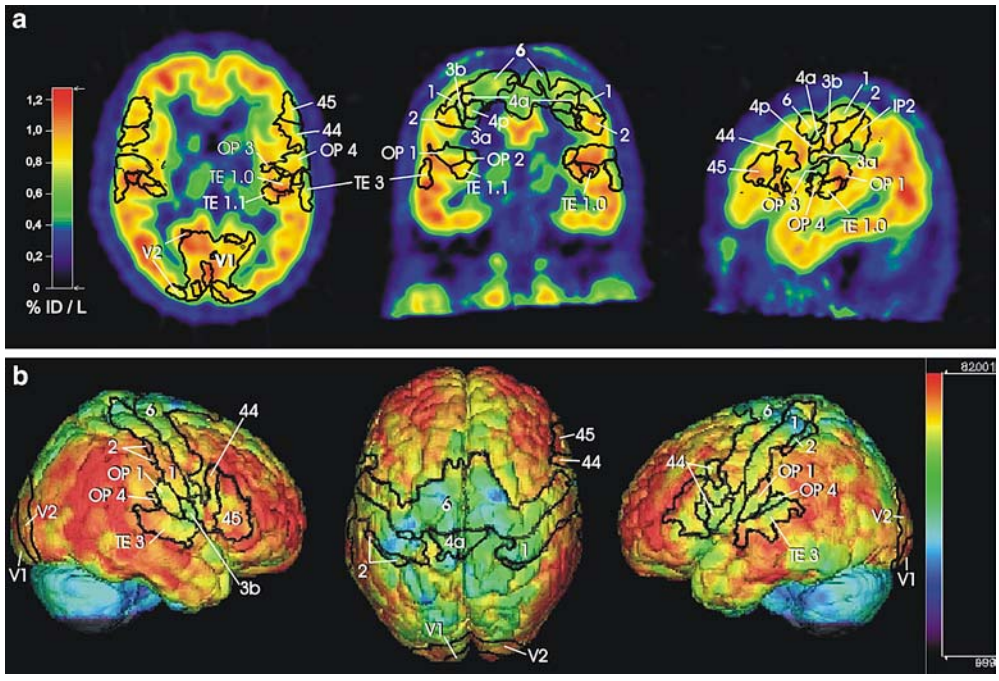

Fig. 1 Superposition of the cytoarchitectonic maximum probability atlas onto functional PET data as exemplified in subject 2 (sum of 11 frames, 5–60 min, rainbow + black-scaled). Numbers of Brodman areas are indicated. **a** Three orthogonal cross-sectional planes. **b** Projection of PET data (maximum intensity across 6 mm) onto the three-dimensionally rendered MNI single subject brain

uptake of the blood–brain barrier penetrating labelled metabolites [^{18}F]altanserinol and [^{18}F](4-fluorophenyl)-pyridine and (b) non-specific binding of [^{18}F]altanserin itself (Price et al. 2001a, 2001b; Tan et al. 1999). As these effects also occur in the reference region (cerebellum), 5-HT$_{2A}$ receptor density tends to be underesti-

Table 1 Distribution volume ratios (DVRs) of 2×19 cytoarchitectonic maximum probability maps (*MPMs*) as obtained from forward and backward normalization procedures and receptor densities from in vitro autoradiography of 11 corresponding cytoarchitectonic regions

Area	PET DVR ($n = 5$; two female; mean age = 23.2 years)							Autoradiography (fmol/g)		
	Forward procedure			Backward procedure			Difference forward–backward (%)			
	Volume (r/l)	Mean (r/l)	SD (r/l)	Volume (r/l)	Mean (r/l)	SD (r/l)		N^a	Mean	SD
BA1	5.7/7.3	2.1/1.9	0.29/0.24	4.5/6.4	1.9/1.7	0.20/0.08	9.3/7.3	3/4	384	136
BA2	8.0/8.4	2.2/2.3	0.18/0.18	6.5/7.0	2.3/2.3	0.21/0.20	−5.8/−1.7	3/4	428	155
BA3b	6.8/4.7	2.1/2.2	0.19/0.20	5.8/4.8	2.2/2.2	0.27/0.21	−3.4/0.3	3/4	440	173
BA4a	9.9/10.2	1.8/1.8	0.29/0.28	8.6/7.7	1.8/1.8	0.18/0.22	1.1/0.7			
BA4p	3.3/3.9	1.7/1.8	0.26/0.12	2.4/3.1	2.0/1.9	0.16/0.15	−14.9/−7.6			
BA4		1.8	0.26		1.9	0.19	−2.2	3/4	289	93
BA6	34.1/32.4	2.0/2.0	0.23/0.25	27.9/26.3	1.9/1.9	0.24/0.21	4.9/ 3.0	2/3	327	216
V1	19.8/20.8	2.3/2.3	0.10/0.11	15.9/16.4	2.3/2.3	0.15/0.18	1.3/2.1	2/3	451	204
V2	13.0/11.1	2.3/2.2	0.10/0.11	11.5/10.1	2.2/2.2	0.13/0.15	4.4/ 2.3	2/3	414	151
TE 1.0[b]	1.9/1.6	2.6/2.6	0.29/0.26	1.7/1.3	2.7/2.7	0.30/0.42	−1.4/−4.4			
TE 1.1[b]	1.3/1.2	2.2/2.3	0.14/0.27	1.1/1.0	2.2/2.2	0.22/0.42	−0.1/4.7			
BA41		2.4	0.25		2.5	0.34	−0.7	3/4	432	216
TE3	6.0/6.5	2.3/2.3	0.19/0.16	5.2/5.7	2.3/2.4	0.24/0.15	−0.3/−3.6	3/4	417	135
BA44	6.6/9.4	2.6/2.4	0.20/0.23	5.6/8.0	2.6/2.4	0.25/0.23	−0.9/−2.8	1/2	176	13
BA45	8.1/6.6	2.5/2.3	0.18/0.22	7.0/6.1	2.5/2.4	0.22/0.22	−1.0/−2.1	1/2	145	52
IP2[b]	0.8/2.4	2.8/2.3	0.29/0.23	0.5/2.1	2.8/2.4	0.33/0.19	1.1/−2.4			
IP1[b]	0.9/2.7	1.8/2.1	0.38/0.36	0.8/2.2	2.3/2.4	0.37/0.35	−23.0/−10.9			
OP1[b]	4.8/5.6	2.5/2.4	0.11/0.13	3.8/5.0	2.5/2.5	0.13/0.15	−0.3/−0.8			
OP2[b]	1.2/1.7	2.0/2.1	0.17/0.28	1.0/0.9	1.9/1.9	0.18/0.38	7.4/10.7			
OP3[b]	1.7/1.8	1.8/1.9	0.27/0.13	1.6/1.8	1.9/1.9	0.21/0.17	−5.1/2.4			
OP4[b]	3.8/4.7	2.4/2.2	0.26/0.22	3.2/4.0	2.4/2.3	0.23/0.18	−2.5/−3.1			
Group	282.6	2.150	0.197	234.6	2.142	0.199	0.4			

Given mean values (BA4, BA41, group) are volume-weighted.
r right, *l* left, *SD* standard deviation

[a] Number of subjects/number of hemispheres $n = 4$: all hemispheres; $n = 3$, BA6 from hemispheres 1, 3l, 3r; BA17 and BA18 from hemispheres 2, 3r, 3l, $n = 2$: hemispheres 3r and 3l

[b] TE 1.0 and TE 1.1 are subareas of BA41, TE3 partially overlaps with BA42; IP1 and IP2: ventral and anterior intraparietal area; OP1-4 correspond to the functionally defined secondary somatosensory cortex, V1 and V2 are homologous to BA17 and BA18, respectively

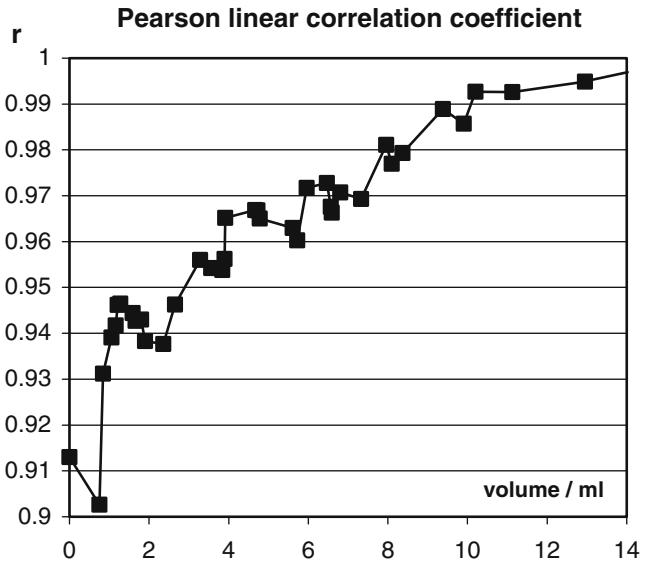

Fig. 2 Correlation between distribution volume ratios (*DVRs*) obtained from the forward and backward normalization procedures in dependency of the volume of the smallest region. Iterative removal of the smallest region results in a correlation coefficient exceeding 0.95 for regions larger than 3.5 ml and 0.975 for regions larger than 8 ml

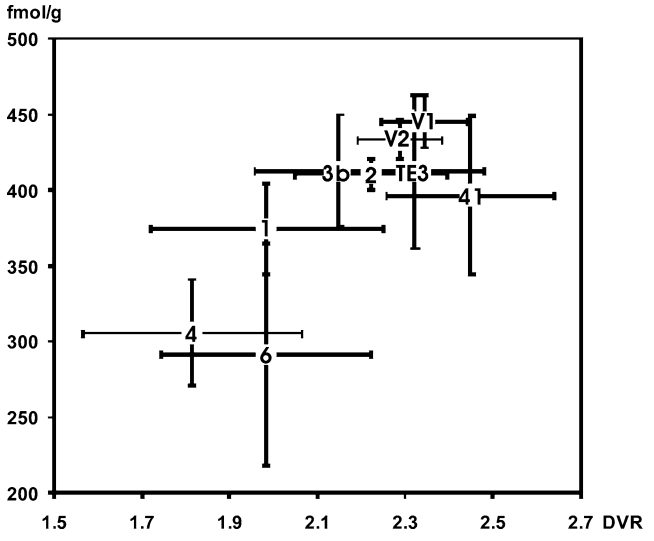

Fig. 3 Scatter plot of the relation of PET data obtained from the forward procedure to linearly normalized receptor densities (fmol/g) obtained from postmortem autoradiography for nine corresponding cytoarchitectonic regions: BA1, 2, 3b, 4, 6, V1, V2, BA41, TE3. Standard deviations are indicated by *vertical and horizontal bars*

mated by DVR measurements. Furthermore, the PET signal is dispersed due to partial volume effects.

Since spatial resolution of PET is limited, attempts have been made to determine the critical ROI size for PET analysis. In a methodological study on cylindrical objects, Hoffman et al. (1979) found an object size of 1.5×FWHM (full width of half maximum) in each direction (*x*,*y* and *z*) to yield a recovery of object radioactivity with recovery co-efficiants (RC) higher than 95%. In our setting, this would correspond to a volume of 0.5 ml. Because cortical areas are not cylindrical, the relation of volume to VOI surface may represent an adequate parameter to characterize a VOI's shape. However, VOI surface is not easy to assess by means of standard software. In order to identify those MPMs from the atlas, which are large enough to enable stable PET analysis, we arranged MPMs by volume and calculated interprocedure correlation coefficients by iteratively removing the smallest MPMs. At a volume of ≥3.5 ml, the interprocedure correlation co-efficient exceeded 0.95. As there was some interindividual variation of the interprocedure correlation, it appears useful to check forward and backward results to control for suboptimal outcome due to atypical brain morphology. Note that the outcome of normalization, and resulting DVR differences, may be biased due to the localization of some regions in a sulcus (e.g., BA3a, OP2, and IP1). This is particularly relevant to BA3a, thus explaining its artificial white matter position after normalization to the single-subject template. Suboptimal overlay of PET and atlas in subject 4 may result from an atypical distribution of cytoarchitectonic regions across gyri and sulci in this subject.

Consistent with the literature (e.g., Pazos 1987; Adams et al. 2004), in both PET and autoradiography radioligand binding was highest in BA17 and BA18 and lowest in BA4 and BA6. The relatively low correlation between PET and autoradiography data seems

Table 2 Pearson linear correlation coefficients (**a**) between forward and backward normalization procedures and (**b**) between each procedure and linearly normalized autoradiography (9 of 11 regions, i.e. BA1, BA2, BA3b, BA4, BA6, V1, V2, BA41, and TE3)

Correlation coefficients (subject)	PET to PET* (all 38 regions) (forward to backward)	PET to mean autoradiography** (9 of 11 regions)	
		Forward procedure	Backward procedure
1	0.85	0.52	0.47
2	0.95	0.65	0.48
3	0.96	0.55	0.55
4	0.55	0.38	0.37
5	0.70	0.80***	0.65***
Mean	0.89	0.64	0.47

*Pearson's linear correlation coefficient; **Spearman's rank correlation coefficient; *** $p < 0.05$

to question the validity of our approach; however, note that sample sizes were small, and the number of regions entered into statistical comparison was further reduced by a lack of autoradiographic data. A priori exclusion of areas BA44 and 45 from in vivo–in vitro comparison was necessary, because in vitro data were available from one subject only. Furthermore, regional differences in age-related decline of [^{18}F]altanserin binding (Adams et al. 2004: similar decline for ventrolateral frontal, superior temporal and sensorimotor areas, but low decline for occipital areas) could account for a non-linear distortion of the regional pattern of [^{18}F]altanserin binding. A higher correlation of autoradiography and PET data could be achieved by applying partial volume correction (Koepp et al. 1989), age-mached comparison groups, and larger VOIs.

In conclusion, the application of cytoarchitectonic MPMs for the a priori definition of VOIs in neuroreceptor PET analysis is feasible. By accounting for the cytoarchitectonic organization of the cerebral cortex and by avoiding observer-dependent bias, the suggested atlas approach is superior to a manual definition of VOIs. This advantage is of particular relevance to studies of clinical populations that show normal morphological indices, but focal neurochemical abnormalities.

Acknowledgements This study was part of the German Research Network on Schizophrenia funded by the German Federal Ministry for Education and Research (BMBF). Further support was received from the Deutsche Forschungsgemeinschaft (DFG) (Klinische Forschergruppe 112 to Karl Zilles and Andreas Bauer) and the International Consortium for Brain Mapping (ICBM). René Hurlemann and Andreas Matusch contributed equally to the study. The authors thank H. Herzog, L. Tellmann, S. Schaden, E. Theelen (PET group), B. Elghahwagi, G. Oefler, and J.N. Shah (MRI group) as well as M. Lang, B. Palm, E. Wabbals, and K. Hamacher (Cyclotron and Radiosynthesis Group, Institute of Nuclear Chemistry, Research Center Jülich) for excellent technical support.

References

Abi-Dargham A, Laruelle M, Seibl J, Rattner Z, Baldwin RM, Zoghbi SS, Zea-Ponce Y, Bremmer JD, Hyde TM, Charney DS, Hoffer PB, Innis RB (1994) SPECT Measurement of benzodiazepine receptors in human brain with iodine-123-iomazenil: kinetic and equilibrium paradigms. J Nucl Med 35:228–238

Adams KH, Pinborg LH, Svarer C, Hasselbalch SG, Holm S, Haugbol S, Madsen K, Frokjaer V, Martiny L, Paulson OB, Knudsen GM (2004) A database of [(18)F]-altanserin binding to 5-HT(2A) receptors in normal volunteers: normative data and relationship to physiological and demographic variables. Neuroimage 21:1105–1113

Amunts K, Schleicher A, Buergel U, Mohlberg H, Uylings HBM, Zilles K (1999) Broca's region revisited: cytoarchitecture and intersubject variability. J Comp Neurol 412:319–341

Amunts K, Malikovic A, Mohlberg H, Schormann T, Zilles K (2000) Brodmann's areas 17 and 18 brought into stereotaxic space—where and how variable? Neuroimage 11:66–84

Amunts K, Schleicher A, Zilles K (2002) Architectonic mapping of human cerebral cortex. In: Schütz A, Miller R (eds) Cortical areas: unity and diversity. Herwood Academic Publishers, pp 29–521.

Choi HJ, Amunts K, Mohlberg H, Fink GR, Schleicher A, Zilles K (2002) Cytoarchitectonic mapping of the anterior ventral bank of the intraparietal sulcus in humans. Human brain mapping 2002 meeting. Neuroimage 16:S591

Collins DL, Neelin P, Peters TM, Evans AC (1994) Automatic 3D intersubject registration of MR volumetric data in standardized Talairach space. J Comp Assist Tomogr 18:192–205

Eickhoff S, Walters NB, Schleicher A, Krill J, Egan GF, Zilles K, Watson JDG, Amunts K (2004) High-resolution MRI reflects myeloarchitecture and cytoarchitecture of human cerebral cortex. Hum Brain Mapp 24:206–215

Eickhoff S, Mohlerg H, Stephan KE, Fink GR, Zilles K, Amunts K (2004) A new SPM toolbox for the combined analysis of fMRI data and probabilistic cytoarchitectonic maps. Human brain mapping 2004 meeting, Poster No. WE 167

Eickhoff S, Schleicher A, Zilles K, Amunts K (2005b) The human parietal operculum. I. Cytoarchitectonic mapping of subdivisions. Cerebral Cortex (in press)

Eickhoff S, Amunts K, Mohlberg H, Zilles K (2005a) The human parietal operculum II. Stereotaxic maps and correlation with functional imaging results. Cerebral Cortex (in press)

Evans AC, Collins DL, Mills SR, Brown ED, Kelly RL, Peters TM (1993) 3D statistical neuroanatomical models from 305 MRI volumes. In: Nuclear science symposium and medical imaging conference, 1993 IEEE conference record 3, pp 1813–1817

Geyer S, Ledberg A, Schleicher A, Kinomura S, Schormann T, Buergel U, Klingberg T, Larsson J, Zilles K, Roland PE (1996) Two different areas within the primary motor cortex of man. Nature 382:805–807

Geyer S, Schleicher A, Zilles K (1999) Area 3a, 3b, and 1 of human primary somatosensory cortex: 1. Microstructural organization and interindividual variability. Neuroimage 10:63–83

Geyer S, Schormann T, Mohlberg H, Zilles K (2000) Areas 3a, 3b, and 1 of human primary somatosensory cortex: 2. Spatial normalization to standard anatomical space. Neuroimage 11:684–696

Geyer S, Schleicher A, Schormann T, Mohlberg H, Bodegard A, Roland PE, Zilles K (2001) Integration of microstructural and functional aspects of human somatosensory areas 3a, 3b, and 1 on the basis of a computerized brain atlas. Anat Embryol (Berl) 204:351–366

Grefkes C, Geyer S, Schormann T, Roland P, Zilles K (2001) Human somatosensory area 2: observer-independent cytoarchitectonic mapping, interindividual variability, and population map. Neuroimage 14:617–631

Hamacher K, Hamkens W (1995) Remote controlled one step production of ^{18}F labeled butyrophenone neuroleptics exemplified by the synthesis of n.c.a. [18F]N-methyl-spiperone. Appl Radiat Isot 46:911–916

Hoffman EJ, Huang SC, Phelps ME (1979) Quantitation in positron emission computed tomography: 1. Effects of object size. J Comput Assist Tomogr 3:299–308

Holmes CJ, Hoge R, Collins L, Woods R, Toga AW, Evans AC (1998) Enhancement of MR images using registration for signal averaging. J Comput Assist Tomogr 22:324–333

Koepp MJ, Hand KS, Labbe C, Richardson MP, Van Paesschen W, Baird VH, Cunningham VJ, Bowery NG, Brooks DJ, Duncan JS (1998) In vivo [11C]flumazenil-PET correlates with ex vivo [3H]flumazenil autoradiography in hippocampal sclerosis. Ann Neurol 43:618–626

Laruelle M, Baldwin RM, Rattner Z, Al-Tikriti MS, Zea-Ponce Y, Zoghbi SS, Charney DS, Price JC, Frost JJ, Hoffer PB, Innis RB (1994) J Cereb Blood Flow Metab 14:439–452

Lemaire C, Cantineau R, Guillaume M, Pleneveaux A, Christiaens L (1991) Fluorine-18-Altanserin: a radioligand for the study of serotonin receptors with PET: radiolabeling and in vivo biologic behavior in rats. J Nucl Med 32:2266–2272

Logan J, Fowler JS, Volkow ND, Wang GJ, Ding YS, Alexoff DL (1996) Distribution volume ratios without blood sampling from graphical analysis of PET data. J Cereb Blood Flow Metab 16:834–840

Mohlberg H, Evans AC, Lerch J, Amunts K, Zilles K (2003) Probabilistic cytoarchitectonic maps transformed into MNI space. Human brain mapping 2003 meeting. NeuroImage 19:S905

Morosan P, Rademacher J, Schleicher A, Amunts K, Schormann T, Zilles K (2001) Human primary auditory cortex: cytoarchitectonic subdivisions and mapping into a spatial reference system. Neuroimage 13:684–701

Morosan P, Rademacher J, Palomero-Gallagher N, Zilles K (2005) Anatomical organization of the human auditory cortex: cytoarchitecture and transmitter receptors. In: Heil, König, Budinger (eds) Auditory cortex: towards a synthesis of human and animal research. Lawrence Erlbaum, Mahwah, NJ

Pazos A, Probst A, Palacios JM (1987) Serotonin receptors in the human brain—IV. Autoradiographic mapping of serotonin-2 receptors. Neuroscience 21:123–139

Price JC, Lopresti BJ, Mason NS, Holt DP, Huang Y, Mathis CA (2001a) Analyses of [(18)F] altanserin bolus injection PET data. I: consideration of radiolabeled metabolites in baboons. Synapse 41:1–10

Price JC, Lopresti BJ, Meltzer CC, Smith GS, Mason NS, Huang Y, Holt DP, Gunn RN, Mathis CA (2001b) Analyses of [(18)F]altanserin bolus injection PET data. II: consideration of radiolabeled metabolites in humans. Synapse 41:11–21

Schleicher A, Amunts K, Geyer S, Morosan P, Zilles K (1999) Observer-independent method for microstructural parcellation of cerebral cortex: a quantitative approach to cytoarchitectonics. Neuroimage 9:165–177

Tan PZ, Baldwin RM, VanDyck CH, Al-Tikriti M, Roth B, Khan N, Charney DS,Innis RB (1999) Characterization of radioactive metabolites of 5-HT2A-receptor PET ligand [^{18}F]altanserin in human and rodent. Nuclear Med Biol 26:601–608

Zilles K, Palomero-Gallagher N, Grefkes C, Scheperjans F, Boy C, Amunts K, Schleicher A (2002) Architectonics of the human cerebral cortex and transmitter receptor fingerprints: reconciling functional neuroanatomy and neurochemistry. Eur Neuropsychopharmacol 12:587–599

Zilles K, Schleicher A, Palomero-Gallagher N, Amunts K (2002) Quantitative analysis of cyto- and receptor architecture of the human brain. In: Mazziotta JC, Toga A (eds) Brain mapping: the methods. Elsevier, NY, pp 573–602